nature physics

LETTERS

https://doi.org/10.1038/s41567-021-01275-3

Check for updates

OPEN

# Nonlinear second-order photonic topological insulators

Marco S. Kirsch[1,6], Yiqi Zhang[2,6], Mark Kremer[1], Lukas J. Maczewsky[1], Sergey K. Ivanov[3,4], Yaroslav V. Kartashov[3,5], Lluis Torner[5], Dieter Bauer[1], Alexander Szameit[1]✉ and Matthias Heinrich[1]

**Higher-order topological insulators are a novel topological phase beyond the framework of conventional bulk–boundary correspondence[1,2]. In these peculiar systems, the topologically non-trivial boundary modes are characterized by a co-dimension of at least two[3,4]. Despite several promising preliminary considerations regarding the impact of nonlinearity in such systems[5,6], the flourishing field of experimental higher-order topological insulator research has thus far been confined to the linear evolution of topological states. As such, the observation of the interplay between nonlinearity and the dynamics of higher-order topological phases in conservative systems remains elusive. Here we experimentally demonstrate nonlinear higher-order topological corner states. Our photonic platform enables us to observe nonlinear topological corner states as well as the formation of solitons in such topological structures. Our work paves the way towards the exploration of topological properties of matter in the nonlinear regime, and may herald a new class of compact devices that harnesses the intriguing features of topology in an on-demand fashion.**

Topological insulators are a recently discovered state of matter. Among their unique features are chiral surface currents that are topologically protected from scattering at defects and disorder, while the bulk material remains insulating[7]. Soon after the first experimental realizations in condensed matter systems, topological notions proliferated across other fields of physics, resulting in the experimental demonstrations of topological dynamics in various platforms, particularly in photonics[8,9]. Recently, as a generalization to these concepts, the existence of higher-order topological insulators (HOTIs) was proposed[1,10,11] and experimentally demonstrated in solid-state systems[12] as well as a plethora of other platforms, including acoustics[13–15] and photonics[16–18]. In this new type of topological phase, the dimensionality of the topologically non-trivial boundary modes is more than one dimension below that of the bulk. In other words, a $d$-dimensional $n$th-order topological insulator supports $(d-n)$-dimensional boundary states[4] (Fig. 1a). Although the study of HOTIs is still in its infancy, the applicative potential of these systems has been widely recognized, for example, for robust low-loss cavities[19] that harness the unusually strong modal confinement of corner states. Moreover, HOTIs are also related to real-space topological defects such as lattice disclinations[20], which may enable the realization of Majorana bound states and non-Abelian braiding statistics[21].

Despite a number of promising preliminary theoretical considerations[6,22,23], several experimental studies in dissipative HOTI systems[24–26], as well as the recently demonstrated potential of harnessing tightly localized HOTI corner states for the enhancement of nonlinear processes such as third-harmonic generation[27], there is only one experimental study at hand, where the evidence of switching into the HOTI phase under the nonlinear action of a homogeneous global pump was reported in electronic circuits[5]. Importantly, to date, research into the wave dynamics of photonic HOTIs in conservative optical systems has been confined to strictly linear conditions, and their extension in the presence of nonlinear self-action has yet to be explored. Yet, even these first glimpses into the nonlinear regime raise various intriguing fundamental questions. In particular, as the concept of band topology has thus far been considered to be inherently tied to linear systems, the generalization to nonlinear systems is by no means straightforward. Since topological properties can indeed persist in the presence of nonlinearity[28], and may even be established by it[29,30], does the same hold true for HOTIs?

In this work, we experimentally explore the nonlinear dynamics of light in photonic HOTIs based on the kagome geometry (Fig. 1b). The topological phase of this lattice type is characterized by the corresponding topological invariants—two bulk polarizations, namely, $\mathcal{P}_x = \mathcal{P}_y = \frac{1}{3}$ (refs. [6,18,31]). We observe the emergence of nonlinear topological corner states as they bifurcate from their linear counterpart, as well as the formation of spatial solitons in such structures. To this end, we employ lattices of evanescently coupled optical waveguides, characterized by a focusing Kerr response, as a versatile testbed for nonlinear physics[28,30,32].

The wave dynamics in our system obey the normalized continuous nonlinear Schrödinger equation for the dimensionless light field amplitude $q$ propagating along the normalized longitudinal coordinate $\zeta$:

$$\mathrm{i}\frac{\partial q}{\partial \zeta} = -\frac{1}{2}\left(\frac{\partial^2}{\partial \xi^2} + \frac{\partial^2}{\partial \eta^2}\right) q - |q|^2 q - pR(\xi,\eta)q. \qquad (1)$$

Here $\xi$ and $\eta$ are the normalized transverse coordinates, parameter $p$ describes the contrast of the refractive index modulation, and the lattice profile itself is characterized by the function $R(\xi, \eta)$. The expression $|q|^2 q$ describes the intensity-dependent shift in the local propagation constant as mediated by the action of the Kerr-type nonlinearity[32]. For low input powers, this term is negligible, and

[1]Institut für Physik, Universität Rostock, Rostock, Germany. [2]Key Laboratory for Physical Electronics and Devices of the Ministry of Education & Shaanxi Key Lab of Information Photonic Technique, School of Electronic Science and Engineering, Xi'an Jiaotong University, Xi'an, China. [3]Institute of Spectroscopy, Russian Academy of Sciences, Troitsk, Russia. [4]Moscow Institute of Physics and Technology, Dolgoprudny, Russia. [5]ICFO—Institut de Ciències Fotòniques, The Barcelona Institute of Science and Technology, Castelldefels (Barcelona), Spain. [6]These authors contributed equally: Marco S. Kirsch, Yiqi Zhang. ✉e-mail: alexander.szameit@uni-rostock.de

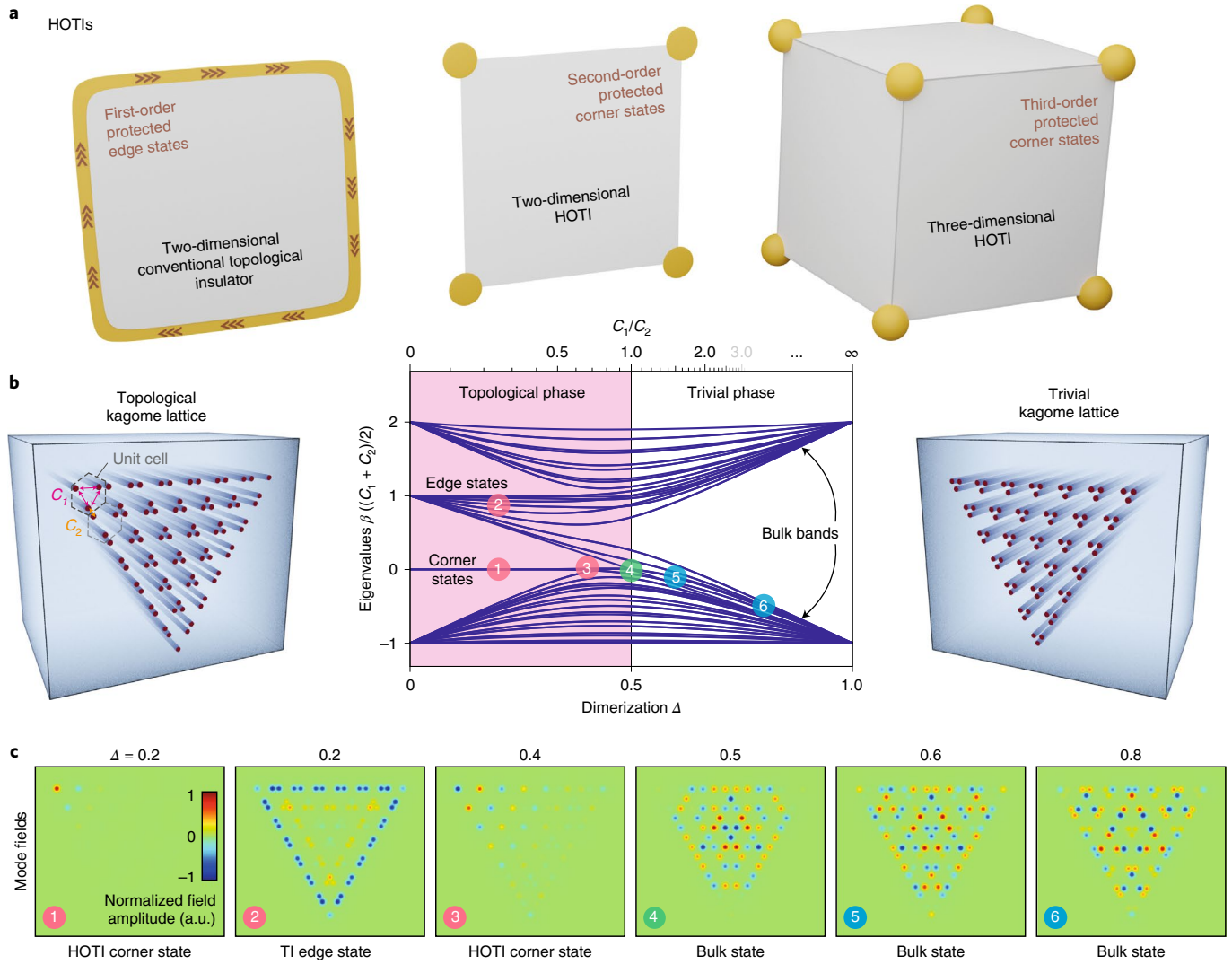


**Fig. 1 | Higher-order topological insulators. a**, In contrast to conventional TIs, HOTIs are topological systems in which protected states exist at lower-dimensional surface features. **b**, The kagome lattice, shown here as a two-dimensional array of waveguides, exhibits a topological phase when coupling $C_2$ between its unit cells exceeds coupling $C_1$ within them, that is, for dimerization $\Delta < 0.5$ (left). By plotting the normalized tight-binding eigenvalues $\beta$ of a triangular kagome lattice as a function of dimerization (middle), the branches associated with both topological edge states and HOTI corner states can be identified. For weak dimerizations, the corner-state branch has not yet emerged from the lower bulk band, placing its constituent non-radiative modes within the continuum of bulk modes[15]. The eigenvalues of the corner modes remain strictly pinned to $\beta = 0$ throughout their domain of existence. Note that the gap of the kagome lattice closes in the undimerized case ($\Delta = 0.5$), and the remaining apparent separation between the bulk bands here is due to the finite size of the model system. In the trivial regime ($\Delta > 0.5$), only the bulk bands exist. **c**, Numerically computed exemplary mode field distributions corresponding to the marked points within the band plot. As an aid to the eye, they have been normalized with respect to their individual maximum absolute values.

the light evolution is effectively linear. For increasing input power, however, the intensity-dependent phases may lead to substantial changes in the propagation dynamics across the lattice sites. We note that equation (1) is formally equivalent to the well-known Gross–Pitaevskii equation, which describes the mean-field evolution of bosonic many-particle quantum systems with inter-particle interaction. In this vein, our classical photonic system also offers a model capable of probing the evolution of many-body quantum states.

The higher-order topological properties of kagome-based arrangements, first experimentally demonstrated in an acoustical context[15], arise from the degree of dimerization of the bond strengths within and between the individual unit cells and are summarized in Fig. 1b. Here we consider a semi-infinite kagome lattice truncated along two intersecting lattice planes such that a 60° corner is formed on its upper left. In Fig. 1b, the limiting cases of dimerization are illustrated. When the intra-cell bond $C_1$ is weaker than the inter-cell bond $C_2$ (Fig. 1b, left), the topological phase of the system is associated with emerging non-trivial polarizations, namely, $\mathcal{P}_x = \mathcal{P}_y = \frac{1}{3}$ (refs. [6,18,31]). The trivial phase—identified by vanishing polarizations $\mathcal{P}_x = \mathcal{P}_y = 0$ (refs. [6,18,31])—occurs when the strength of the intra-cell bond exceeds that of the inter-cell bond ($C_1 < C_2$; Fig. 1b, right). Figure 1b, middle, shows the ensemble of propagation constants $\beta$ (representing the tight-binding eigenvalues of the linear version of equation (1) for a triangular kagome lattice comprising 84 sites) as a function of dimerization. The homogeneous lattice is defined by a value of 0.5 for the dimerization parameter $\Delta = C_1/(C_1 + C_2)$, marking the phase transition between the topological regime ($\Delta < 0.5$) and the trivial one ($\Delta > 0.5$). Exemplary mode fields corresponding to the numbered locations in this 'band structure' are shown in

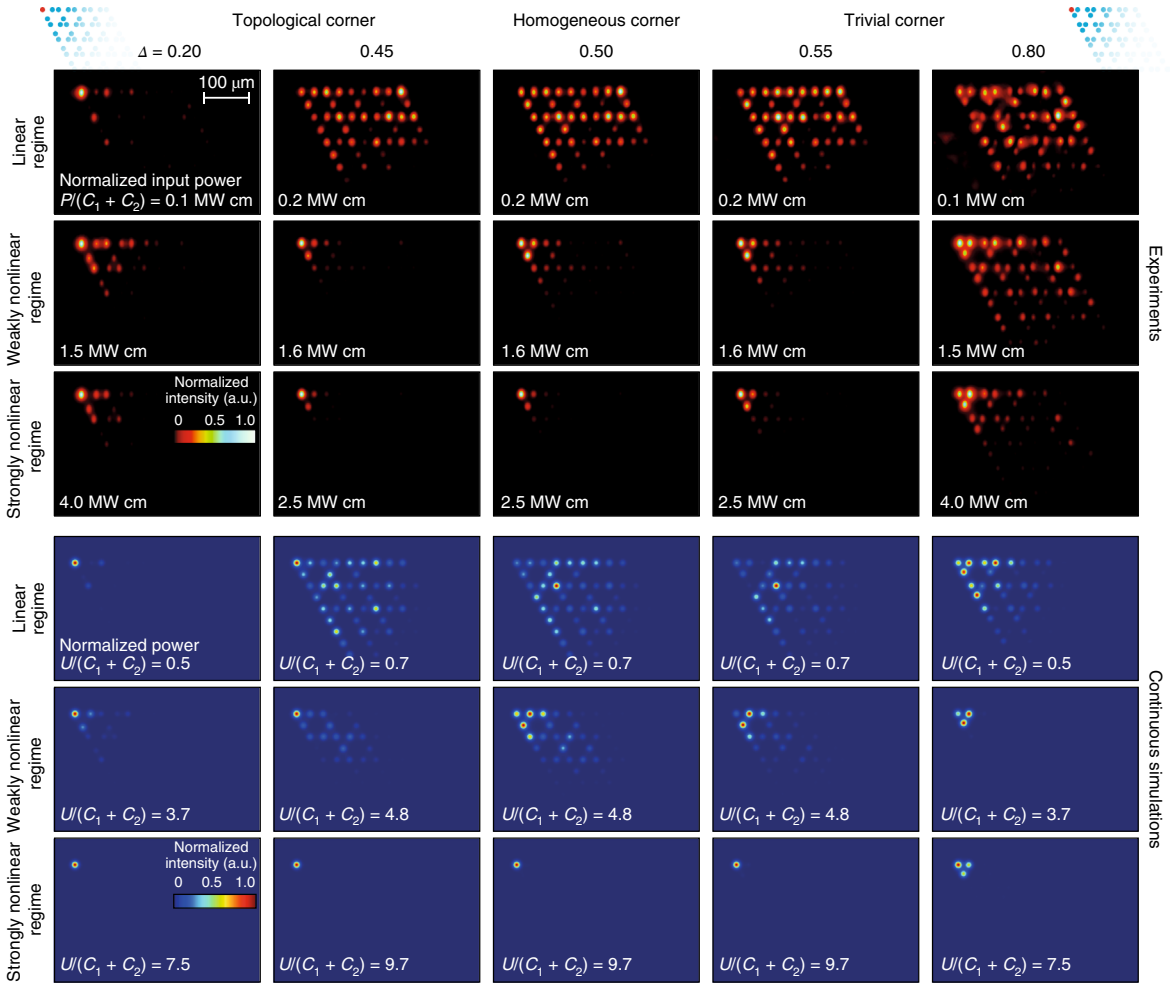


**Fig. 2 | Nonlinear corner excitations in dimerized kagome lattices.** Experimental images are shown in the top three rows, whereas corresponding continuous simulations are shown in the bottom three rows. Given the scaling of the nonlinear response with the overall coupling strength in the system, experimental as well as numerical powers are provided in the normalized form. First column ($\Delta = 0.20$): in the strongly topological regime, linear corner excitations predominantly populate the HOTI state. Increasing the power leads to an intermediate nonlinear phase matching to bulk modes, until at higher powers, a tightly localized corner soliton forms. Second column ($\Delta = 0.45$): since the weakly topological regime features HOTI states that extend far into the lattice (third panel in Fig. 1c), linear corner excitations yield considerable bulk diffraction, and the additional action of nonlinearity is required to form a localized corner state. Nevertheless, this contraction occurs faster than in the trivial case (middle column, $\Delta = 0.50$). The weakly dimerized trivial regime (fourth column, $\Delta = 0.55$) is instead characterized by intra-unit cell dynamics that yield two separate localization steps as the power is increased. In the strongly dimerized trivial regime (fifth column, $\Delta = 0.80$), the intermediate localization in the three guides of the corner unit cell is even more pronounced.

Fig. 1c. Indeed, only the topological regime allows for states whose eigenvalues fall in the topological gap separating the bulk bands of the lattice for $\Delta < 0.5$. However, the branches associated with the conventional topological edge states exhibit a certain slope, and the mid-gap branch is exclusively composed of states residing at the corners of the lattice. It is exactly these corner states that arise due to the higher-order topology of the lattice, and, as such, constitute the defining feature of our second-order photonic topological insulator. Notably, the generalized chiral symmetry of the kagome lattice pins their tight-binding eigenvalues to $\beta = 0$ throughout their domain of existence, and protects them from radiating into the bulk even in the weakly dimerized case when the branch has not yet fully emerged from the bulk band[15]. In contrast to conventional topological insulators, such as insulators with broken time-reversal symmetry supporting chiral currents at their edges, HOTIs may support not only edge or hinge states, but also immobile topological corner modes (Fig. 1a).

To experimentally probe the linear as well as nonlinear dynamics, we fabricated rhomboidal kagome lattices comprising 65 waveguides with the femtosecond laser direct-writing technique, and the corner sites were excited with intense ultrashort laser pulses to provide sufficient peak powers to elicit a nonlinear response. Figure 2 presents an overview of characteristic output patterns obtained from a sample length of 100 mm for different dimerizations and different input powers. In all the cases, light was injected into the upper-left corner site. To ensure a common power scale despite the widely varying absolute coupling values present for the samples with different dimerizations, the injected powers $P_{in}$ are normalized with respect to the sum of the two couplings, that is, $P = P_{in}/(C_1 + C_2)$. The experimentally observed results are shown in the upper three rows of Fig. 2, whereas the lower three rows in Fig. 2 provide the corresponding numerical simulations, where the numerically launched dimensionless power $U_{in}$ is equivalently normalized as $U = U_{in}/(C_1 + C_2)$. In the homogeneous lattice ($\Delta = 0.5$), a linear excitation ($P = 0.2$ MW cm) deeply penetrates into the lattice. When the power is increased to $P = 1.6$ MW cm, a decrease in transverse broadening marks the onset of nonlinearity; at an even higher input power ($P = 2.5$ MW cm), light remains confined to the initially excited waveguide as a tightly localized soliton is formed[33].

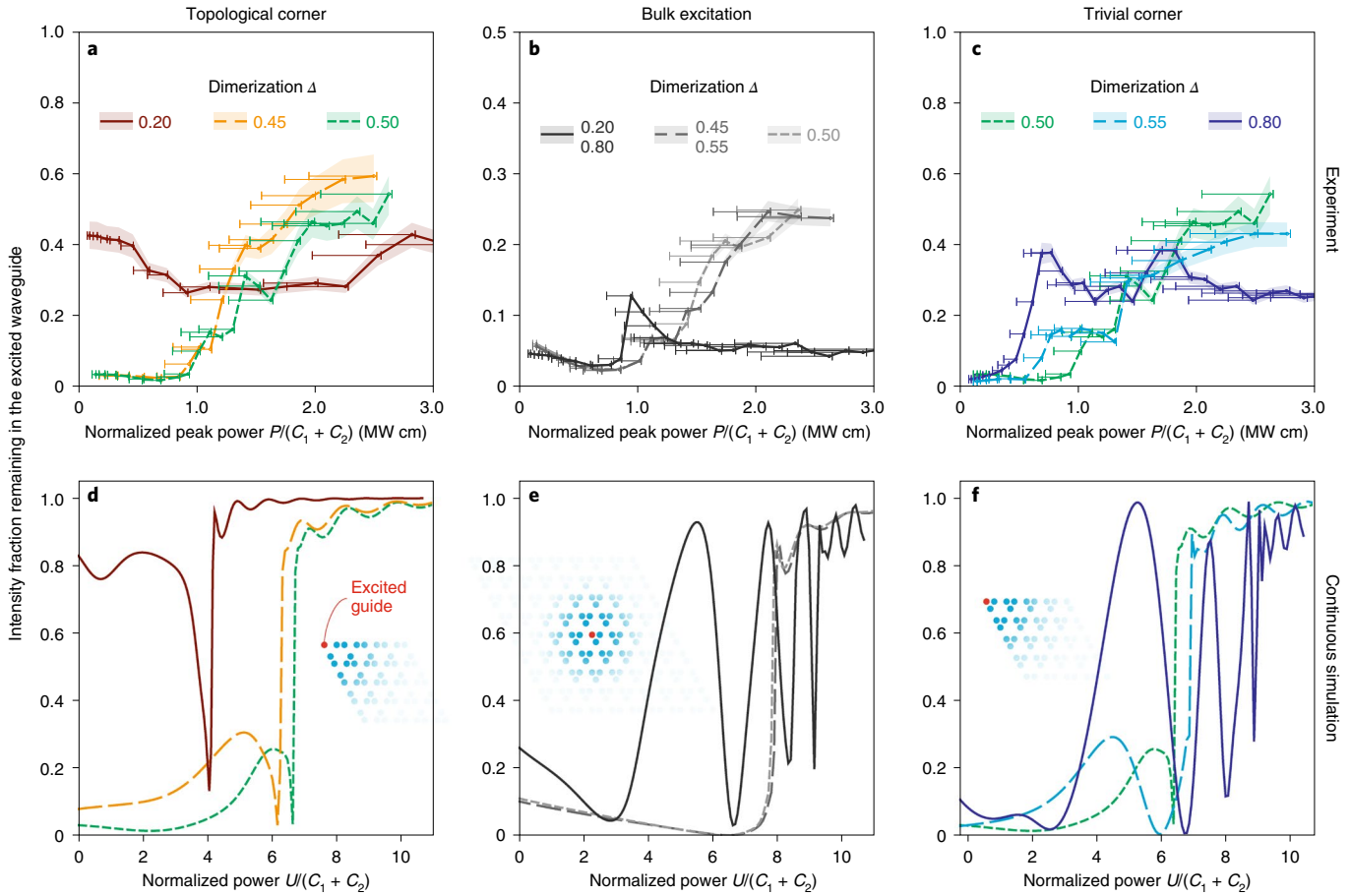


**Fig. 3 | Power-dependent localization in the dimerized kagome lattice. a**, Measured intensity fraction remaining in the topological corner waveguide. In the strongly dimerized case ($\Delta = 0.20$, solid line), nonlinear phase matching to the bulk modes temporarily lifts the topological protection of the corner mode, as evidenced by intermediate delocalization. While the weakly dimerized topological system ($\Delta = 0.45$, long dashed line) does not capture linear single-site excitations at its topological corner, nonlinear localization is accelerated compared with the homogeneous lattice ($\Delta = 0.50$, short dashed line). The ribbons around the graphs represent the range of variation obtained without background subtraction (lower edge) and with twice the background intensity (upper edge) removed from the recorded output patterns. The horizontal error bars represent a relative range of (−22%, +1%), combining the influence of different intensity regimes present in the pulsed excitation as well as ±1% overall pulse energy fluctuations. **b**, Bulk excitations cannot distinguish between the topological and trivial regimes. However, the presence of two distinct coupling values in dimerized systems yields two separate power scales at which partial and full localization occurs. In terms of normalized power, stronger dimerizations lead to an earlier onset of nonlinear dynamics, but require higher powers to fully localize. **c**, A similar two-tiered localization behaviour occurs at trivial corners. **d**–**f**, Corresponding localization plots obtained from continuous numerical simulations. Note that while the linear background inherent in the pulsed excitation scheme employed inevitably smoothes over microscopic details in the experimentally observed localization dynamics, the signatures of localization/delocalization thresholds are faithfully reproduced.

For increasing dimerization ($\Delta > 0.5$), this behaviour remains qualitatively similar, as the lattice continues to reside in the topologically trivial phase with bulk polarizations $\mathcal{P}_x = \mathcal{P}_y = 0$. Linear excitations diffract widely across the lattice, and localization gradually increases with the injected power as the output distribution contracts towards the excited corner, even if the complete collapse onto a single waveguide shifts towards the higher powers necessary to overcome the larger intra-cell coupling $C_2$. This behaviour changes substantially for $\Delta < 0.5$, where the lattice is in the topological phase and $\mathcal{P}_x = \mathcal{P}_y = \frac{1}{3}$. Deeply in the topological phase (at $\Delta = 0.2$), the tightly confined topological corner state captures the vast majority of the launched light, and the bulk of the lattice remains essentially dark. Yet, as the input power is increased, the weakly nonlinear regime ($P = 1.5$ MW cm) actually yields an intermediate delocalization, where nonlinear phase matching to the topological edge states as well as the bulk bands allows a certain fraction of light to escape from the corner. At even higher powers, the strongly nonlinear regime ($P = 4.0$ MW cm) finally serves entirely to trap light in the outermost corner site of the lattice.

Figure 3 depicts the power-dependent localization behaviour in greater resolution. The relative fraction of the overall intensity remaining in the corner waveguide serves as a quantitative measure for the suppression of broadening of the single-site excitation, and it converges to unity for perfect single-site localization. We start our analysis for corner excitations in the lattices with $\Delta > 0.5$ (Fig. 3, right column). The broad linear diffraction patterns at low intensities involve a large portion of the lattice. Increasing the input powers generally leads to increasing localization as the light contracts towards the excited corner site. This is the typical behaviour for two-dimensional corner lattice solitons[33]. Notably, comparing the dimerized cases with the homogeneous lattice, it is evident that the onset of localization systematically occurs at lower powers for larger $\Delta$; at the same time, however, higher powers are required to completely trap light in the corner site, in line with the two characteristic thresholds defined by the powers necessary to overcome the inter- and intra-cell couplings.

When launching light into a bulk site (Fig. 3, middle column), only the deviation from the homogeneous case ($\Delta = 0.50$) matters, as the distinction between inter- and intra-cell couplings

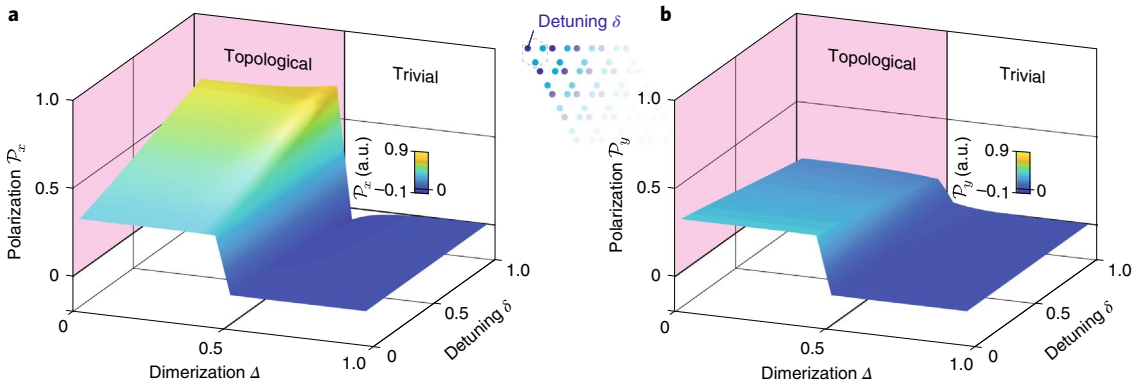


**Fig. 4 | The persistence of topological characteristics in the presence of nonlinear dynamics can be probed by considering a kagome lattice in which one of the three sites of the unit cell features a higher effective index as characterized by detuning $\delta$. a**,**b**, Numerically computed polarizations $\mathcal{P}_x$ (**a**) and $\mathcal{P}_y$ (**b**) that indicate non-trivial topology when assuming positive values. Starting from the characteristic value of $\frac{1}{3}$ in the homogeneous lattice, both $\mathcal{P}_x$ and $\mathcal{P}_y$ experience a characteristic jump at $\Delta = 0.5$, which marks the emergence of a topological corner state even for large detunings ($\delta = 1$). In other words, the corner states in the nonlinear regime continue to be a result of the underlying bulk topology.

is moot in the absence of boundaries. For weakly dimerized lattices ($0.45 < \Delta < 0.55$), light contracts smoothly with increasing power, as the two couplings in the system are of similar magnitude. As a result, the strongly nonlinear regime with its spatial solitons[34] is quickly reached. Instead, strongly dimerized lattices ($\Delta = 0.20$ and $\Delta = 0.80$) once more show an accelerated onset of nonlinear behaviour, while substantially higher powers are required to achieve full localization, as can be seen with particular clarity in the numerical simulations (Fig. 3, bottom row). In the strongly topological regime (Fig. 3, left column), light is indeed strongly localized in the linear regime, as the topological corner states are excited—the hallmark of our second-order topological insulator. When increasing the input power, the localization gradually decreases as the weakly nonlinear corner excitation traverses the window of phase matching with edge and bulk states between $1.0\,\mathrm{MW} < P < 2.5\,\mathrm{MW\,cm}$. Only in the strongly nonlinear regime, when the power ($P > 2.5\,\mathrm{MW\,cm}$) is sufficient to drive the excitation into the semi-infinite gap above the bands of the lattice, a corner soliton forms, and light—once more—localizes in the corner site.

In addition to a phenomenological description of the dynamics, it is important to note that the corner state indeed remains topological—despite the clear imprint of nonlinearity—until the excitation actually enters the band. In other words, for a sizeable range of powers beyond the linear regime ($0\,\mathrm{MW} < P < 1.0\,\mathrm{MW\,cm}$), our system remains a second-order topological insulator, and, as such, continues to support a (nonlinear) topological corner state. This can be framed more formally by the following line of thought. For small dimerizations (for example, $\Delta = 0.2$), the corner state is virtually confined to the outermost unit cell of the topological corner. Therefore, light dynamics in its vicinity are dictated by the local band structure[30,35] that arises from the internal composition of this unit cell. For increasing input powers, self-phase modulation mediated by Kerr nonlinearity systematically increases the effective refractive index of the excited waveguide. Following the notion that only the local band structure (determined by only that part of the system in which light actually resides) determines the light evolution[30,35], one is at liberty to replace the rest of the (unilluminated) lattice with copies of the effectively detuned unit cell. Under the conditions described above, this substitution facilitates the computation of the effective values for polarizations $\mathcal{P}_x$ and $\mathcal{P}_y$ despite the fact the system to be modelled is actually nonlinear. In this vein, we find that the polarizations are no longer pinned to the value of 1/3 associated with identical lattice sites, since chiral symmetry is broken by the detuning. Nevertheless, both polarizations remain strictly positive for $\Delta < 0.5$ (Fig. 4). The fact that $\mathcal{P}_x \neq 0$ and $\mathcal{P}_y \neq 0$ indicates that the existence of the corner states continues to be a result of the underlying bulk topology even in the presence of high input powers.

In summary, we demonstrated a nonlinear photonic second-order topological insulator in a conservative physical system. We systematically explored the features of the underlying lattice in the topological phase, and observed soliton formation as well as nonlinear topological corner states in this structure. Based on an on-chip optical platform, these findings open a new experimental avenue towards developing a more holistic understanding of topological insulators and bringing them to application in future compact devices. Indeed, many fascinating directions of enquiry come to mind: in which ways does the introduction of nonlinearity impact exhibiting fermionic time-reversal symmetry[36]? How can gain, loss and non-Hermiticity, in general, be efficiently harnessed to tailor nonlinear wave-packet evolution[37]? Does the presence of nonlinearity in non-trivial topologies mitigate or—in fact—enhance disorder-induced localization mechanisms[38]? The tools to experimentally tackle these questions are now within reach, and will drive the exploration of the scientific as well as technological aspects of nonlinear topology in all kinds of wave mechanical systems, whether in the photonic, acoustic, optomechanical, polaritonic, atomic or even entirely new domains.

*Note added in proof*: Recently, a manuscript reporting related results was submitted to arXiv[39].

## Online content

Any methods, additional references, Nature Research reporting summaries, source data, extended data, supplementary information, acknowledgements, peer review information; details of author contributions and competing interests; and statements of data and code availability are available at https://doi.org/10.1038/s41567-021-01275-3.

Received: 11 January 2021; Accepted: 20 May 2021;
Published online: 1 July 2021

## References

1. Benalcazar, W. A., Bernevig, B. A. & Hughes, T. L. Quantized electric multipole insulators. *Science* **357**, 61–66 (2017).
2. Langbehn, J., Peng, Y., Trifunovic, L., von Oppen, F. & Brouwer, P. W. Reflection-symmetric second-order topological insulators and superconductors. *Phys. Rev. Lett.* **119**, 246401 (2017).

3. Song, Z., Fang, Z. & Fang, C. ($d-2$)-dimensional edge states of rotation symmetry protected topological states. *Phys. Rev. Lett.* **119**, 246402 (2017).
4. Schindler, F. et al. Higher-order topological insulators. *Sci. Adv.* **4**, eaat0346 (2018).
5. Zangeneh-Nejad, F. & Fleury, R. Nonlinear second-order topological insulators. *Phys. Rev. Lett.* **123**, 053902 (2019).
6. Zhang, Y., Kartashov, Y. V., Torner, L., Li, Y. & Ferrando, A. Nonlinear higher-order polariton topological insulator. *Opt. Lett.* **45**, 4710–4713 (2020).
7. Hasan, M. Z. & Kane, C. L. Colloquium: topological insulators. *Rev. Mod. Phys.* **82**, 3045 (2010).
8. Rechtsman, M. C. et al. Photonic Floquet topological insulators. *Nature* **496**, 196–200 (2013).
9. Hafezi, M., Mittal, S., Fan, J., Migdall, A. & Taylor, J. M. Imaging topological edge states in silicon photonics. *Nat. Photon.* **7**, 1001–1005 (2013).
10. Benalcazar, W. A., Bernevig, B. A. & Hughes, T. L. Electric multipole moments, topological multipole moment pumping, and chiral hinge states in crystalline insulators. *Phys. Rev. B* **96**, 245115 (2017).
11. Ezawa, M. Higher-order topological insulators and semimetals on the breathing kagome and pyrochlore lattices. *Phys. Rev. Lett.* **120**, 026801 (2018).
12. Schindler, F. et al. Higher-order topology in bismuth. *Nat. Phys.* **14**, 918–924 (2018).
13. Ni, X., Gorlach, M., Alù, A. & Khanikaev, A. B. Topological edge states in acoustic kagome lattices. *New J. Phys.* **19**, 055002 (2017).
14. Serra-Garcia, M. et al. Observation of a phononic quadrupole topological insulator. *Nature* **555**, 342–345 (2018).
15. Ni, X., Weiner, M., Alù, A. & Khanikaev, A. B. Observation of higher-order topological acoustic states protected by generalized chiral symmetry. *Nat. Mater.* **18**, 113–120 (2019).
16. Noh, J. et al. Topological protection of photonic mid-gap defect modes. *Nat. Photon.* **12**, 408–415 (2018).
17. Mittal, S. et al. Photonic quadrupole topological phases. *Nat. Photon.* **13**, 692–696 (2019).
18. Li, M. et al. Higher-order topological states in photonic kagome crystals with long-range interactions. *Nat. Photon.* **14**, 89–94 (2020).
19. Ota, Y. et al. Photonic crystal nanocavity based on a topological corner state. *Optica* **6**, 786–789 (2019).
20. Liu, Y. et al. Bulk–disclination correspondence in topological crystalline insulators. *Nature* **589**, 381–385 (2021).
21. Hsu, C.-H., Stano, P., Klinovaja, J. & Loss, D. Majorana Kramers pairs in higher-order topological insulators. *Phys. Rev. Lett.* **121**, 196801 (2018).
22. Tao, Y.-L., Dai, N., Yang, Y.-B., Zheng, Q.-B. & Xu, Y. Hinge solitons in three-dimensional second-order topological insulators. *New J. Phys.* **22**, 103058 (2020).
23. Banerjee, R., Mandal, S. & Liew, T. C. H. Coupling between exciton-polariton corner modes through edge states. *Phys. Rev. Lett.* **124**, 063901 (2020).
24. Zhang, W. X. et al. Low-threshold topological nanolasers based on second-order corner state. *Light Sci. Appl.* **9**, 109 (2020).
25. Han, C., Kang, M. & Jeon, H. Lasing at multidimensional topological states in a two-dimensional photonic crystal structure. *ACS Photonics* **7**, 2027–2036 (2020).
26. Kim, H.-R. et al. Multipolar lasing modes from topological corner states. *Nat. Commun.* **11**, 5758 (2020).
27. Kruk, S. et al. Nonlinear imaging of nanoscale topological corner states. *Nano Lett.* **21**, 4592–4597 (2021).
28. Mukherjee, S. & Rechtsman, M. C. Observation of Floquet solitons in a topological bandgap. *Science* **368**, 856–859 (2020).
29. Hadad, Y., Soric, J. C., Khanikaev, A. B. & Alù, A. Self-induced topological protection in nonlinear circuit arrays. *Nat. Electron.* **1**, 178–182 (2018).
30. Maczewsky, L. J. et al. Nonlinearity-induced photonic topological insulator. *Science* **370**, 701–704 (2020).
31. King-Smith, R. D. & Vanderbilt, D. Theory of polarization of crystalline solids. *Phys. Rev. B* **47**, 1651 (1993).
32. Szameit, A. et al. Discrete nonlinear localization in femtosecond laser written waveguides in fused silica. *Opt. Express* **13**, 10552–10557 (2005).
33. Szameit, A. et al. Observation of two-dimensional surface solitons in asymmetric waveguide arrays. *Phys. Rev. Lett.* **98**, 173903 (2007).
34. Fleischer, J. W., Segev, M., Efremidis, N. K. & Christodoulides, D. N. Observation of two-dimensional discrete solitons in optically induced nonlinear photonic lattices. *Nature* **422**, 147–150 (2003).
35. Hadad, Y., Khanikaev, A. B. & Alù, A. Self-induced topological transitions and edge states supported by nonlinear staggered potentials. *Phys. Rev. B* **93**, 155112 (2016).
36. Maczewsky, L. J. et al. Fermionic time-reversal symmetry in a photonic topological insulator. *Nat. Mater.* **19**, 855–860 (2020).
37. Bandres, M. A. et al. Topological insulator laser: experiments. *Science* **359**, eaar4005 (2018).
38. Stützer, S. et al. Photonic topological Anderson insulators. *Nature* **560**, 461–465 (2018).
39. Hu, Z. et al. Nonlinear control of photonic higher-order topological bound states in the continuum. Preprint at https://arxiv.org/abs/2106.00360 (2021).

## Methods

**Waveguide inscription and lattice parameters.** The dimerized kagome lattices employed in our experiments were fabricated by the femtosecond laser direct-writing technique in 100-mm-long fused silica samples (Corning 7980). Pulses from a titanium:sapphire amplifier system (Coherent Vitara S/RegA 9000; carrier wavelength, 800 nm; pulse duration, 140 fs; pulse energy, 400 nJ; repetition rate, 100 kHz) were focused through a microscope objective (×20 and numerical aperture (NA) = 0.35). The sample itself was translated relative to the focus with a high-precision positioning system (AEROTECH ALS180) at 100 mm min$^{-1}$, yielding single-mode waveguides (effective refractive index contrast ~$5\times10^{-4}$; approximate mode field dimensions 12 µm × 20 µm) for the probe wavelength of 800 nm. Waveguide separations between 22.0 µm and 35.7 µm, corresponding to coupling coefficients between 0.20 cm$^{-1}$ and 0.81 cm$^{-1}$, were chosen to implement arrangements with the desired representative dimerizations of $\Delta = 0.20$, 0.45, 0.50, 0.55 and 0.80.

**Sample characterization.** A high-power titanium:sapphire chirped pulse amplification system (Coherent Astrella-F-1K) provided intense 210 fs pulses of up to peak powers of 30 GW with a bandwidth of 30 nm around the probe wavelength of 800 nm and a repetition rate of 1 kHz. A microscope objective (×2.5 and NA = 0.075) was used to inject these pulses into specific lattice sites, and the resulting power-dependent output intensity distributions at the sample end face were imaged onto a charge-coupled device camera (Basler acA1920-155um) by another microscope objective (×4.0 and NA = 0.1).

**Numerical simulations.** To obtain the exact soliton solutions of equation (1), we employed the ansatz $q = u(\xi,\eta)\exp(\mathrm{i}\bar{\beta}\zeta)$, where $u(\xi,\eta)$ is the real-valued function describing transverse field distribution and $\bar{\beta}$ is the propagation constant in the continuous model. Substitution of this expression into equation (1) yields the nonlinear eigenvalue equation $\bar{\beta}u = \left(\partial_\xi^2 + \partial_\eta^2\right)u + |u|^2 u + pR(\xi,\eta)u$, to which we applied the Newton method. In our continuous model, the refractive index distribution of the array was described by the function $R(\xi,\eta) = \sum_{n,m}\mathcal{Q}(\xi-\xi_n, \eta-\eta_m)$, where $\mathcal{Q}(\xi,\eta) = \exp\{-[(\xi^2+\eta^2)/d^2]^2\}$ represents the profiles of individual super-Gaussian waveguides at transverse positions $(\xi_n,\eta_m)$ in the array with normalized width $d = 0.7$. In our simulations, we used 512 × 512 points per integration window of $-20 \le x \le 20$ and $-22 \le y \le 22$, corresponding to approximately 36 mesh points per waveguide in each dimension to accurately capture the details of the refractive index landscape. Similar to the experimental approach, we calibrated the dimerization of our kagome lattices by evaluating the separation-dependent coupling rate for the simplified index profiles. Extended Data Fig. 1 shows the characteristic power–eigenvalue plots of nonlinear stationary states, which were constructed by varying the nonlinear propagation constant $\bar{\beta}$, inserting the solution from the previous step as an initial guess for the optimization to the new nonlinear propagation constant, and evaluating the total power $U = \int |u|^2 \mathrm{d}\xi\mathrm{d}\eta$ contained in the respective solution $u$.

**Polarizations of the detuned lattice.** The topological characterization of kagome-type lattices is based on polarization $\mathcal{P}$ whose components $\mathcal{P}_{x,y}$ can be numerically calculated by evaluating the integral

$$\mathcal{P}_j = -\frac{1}{4\pi^2}\iint_{\mathrm{BZ}} A_j(k)\mathrm{d}k_x\mathrm{d}k_y \text{ with } A_j(k) = -\mathrm{i}\left\langle u\left|\frac{\partial}{\partial k_j}\right|u\right\rangle,$$

over the Brillouin zone (BZ) with the Bloch states $|u\rangle$. of the first band[6], where $j \in \{x,y\}$. The polarization may be understood as a displacement of the Wannier centres[10], which, in turn, leads to localization at the dangling lattice sites at a boundary (also see ref. [15]). In the presence of additional symmetries, this displacement is pinned to a specific value and protected by the underlying symmetry. A local detuning inevitably breaks this symmetry, which means that the polarization is no longer fixed to a specific value. Nevertheless, a rapid change in polarization can be observed when the couplings of a dimerized system are exchanged. This behaviour is inextricably linked to the creation/destruction of a boundary mode.

To account for the influence of nonlinearity, a (linear) detuning $\delta$ is introduced at the site of the unit cell that is excited with a high-power input beam. This approximation is motivated by the consideration that the local band structure describing the dynamics of light[30,35] is in fact determined by only that part of the system in which light actually resides. As shown in Extended Data Fig. 1, for nonlinear corner states below the linear edge-state band, this is indeed only the outermost corner site. In this vein, the unilluminated part of the lattice can be substituted with copies of the effectively detuned unit cell for numerical purposes. The corresponding Hamiltonian of this equivalent system then reads

$$H(k) = \begin{pmatrix} 0 & v + we^{-\mathrm{i}(k_x-k_y)} & v + we^{-\mathrm{i}k_y} \\ v + we^{-\mathrm{i}(k_x-k_y)} & \delta & v + we^{-\mathrm{i}k_x} \\ v + we^{-\mathrm{i}k_y} & v + we^{-\mathrm{i}k_x} & 0 \end{pmatrix},$$

where the wave numbers $k_{x/y}$ are normalized to the lattice constant and chosen along orthogonal directions. For the simulations, the resolution of $k_{x/y}$ along the derivative is chosen to be 3,900 points, and it is 1,300 points along the orthogonal direction.

Analogous to Fig. 1b, Extended Data Fig. 2 illustrates the dimerization dependence of the eigenvalues of modified kagome lattices, where the on-site potential of the upper-left waveguide in each unit cell is detuned. For strong detunings ($\delta > 1$), the detuned corner-state branch generally lies above the undetuned edge band. In contrast, for intermediate detunings (for example, $\delta = 0.5$), the branch associated with states in the detuned corner may actually intersect with the edge band that comprises states residing along the opposite edge. This spatial separation prevents any interaction of the respective states that might otherwise impact the topological protection.

## Data availability

Source data are provided with this paper. The experimental source data can be found at the Rostock University Publication Server repository (https://doi.org/10.18453/rosdok_id00002977).

## Acknowledgements

We thank C. Otto for preparing the high-quality fused silica samples used for the inscription of all photonic structures employed in this work. We acknowledge funding from the Deutsche Forschungsgemeinschaft (grants SCHE 612/6-1, SZ 276/12-1, BL 574/13-1, SZ 276/15-1 and SZ 276/20-1) and Alfried Krupp von Bohlen und Halbach foundation. Y.V.K. acknowledges support from the Russian Foundation for Basic Research (grant 18-502-12080). Y.Z. acknowledges support from the Natural Science Foundation of China (12074308). Y.V.K. and L.T. acknowledge support from the Government of Spain (Severo Ochoa CEX2019-000910-S), Fundació Cellex, Fundació Mir-Puig and Generalitat de Catalunya (CERCA).

## Author contributions

M.S.K., M.H. and L.J.M. designed and fabricated the photonic lattices. M.S.K. and M.H. conducted the experiments. Y.V.K., Y.Z. and S.K.I. were responsible for continuous simulations. M.S.K. carried out the tight-binding simulations. The experimental and numerical data were evaluated by M.S.K., M.H. and L.J.M. D.B. and M.K. devised the method for analysing the topological characteristics in the nonlinear regime and calculated the polarizations. A.S. and L.T. supervised the efforts of their respective groups. All the authors co-wrote the manuscript.

## Competing interests

The authors declare no competing interests.

## Additional information

**Extended data** is available for this paper at https://doi.org/10.1038/s41567-021-01275-3.

**Correspondence and requests for materials** should be addressed to A.S.

**Peer review information** *Nature Physics* thanks Mercedeh Khajavikhan, Alexander Khanikaev and the other, anonymous, reviewer(s) for their contribution to the peer review of this work.

**Reprints and permissions information** is available at www.nature.com/reprints.

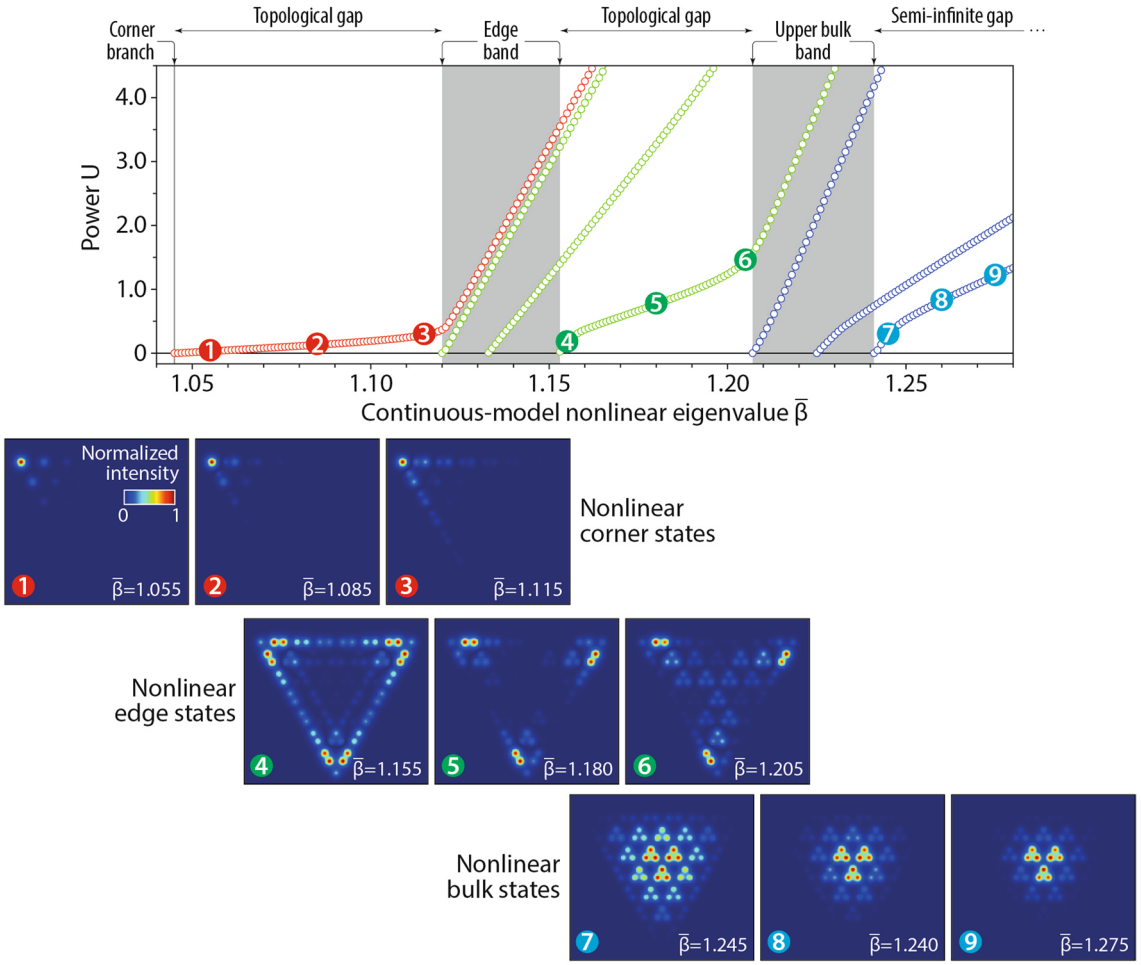


**Extended Data Fig. 1 | Numerically calculated power-eigenvalue-plots and representative intensity profiles of nonlinear stationary solutions in a triangular topological Kagome lattice.** Numerically calculated power-eigenvalue-plots and representative intensity profiles of nonlinear stationary solutions in a triangular topological Kagome lattice with $\Delta = 0.2$ and 84 sites. Note that in the continuous model employed for these calculations, the linear corner mode branch resides at $\bar{\beta} \approx 1.045$, corresponding to a normalized tight-binding eigenvalue of $\beta = 0$. The normalized intensity profiles of representative mode fields for nonlinear corner, edge and bulk states are shown as panels "1"-"9", corresponding to the respectively marked points in the main plot. The power contained in the nonlinear corner state (red trace) increases proportionally with $\bar{\beta}$, indicating that the shape of the distribution does not change substantially as the nonlinear mode approaches the edge band – in other words, the mode remains tightly localized in the corner site (cf. "1"-"3"). Within the edge band, hybridization with nonlinear edge states (green traces) suddenly increases the slope of the branch, which is consistent with the intermediate regime of delocalization observed in our experiments (see Fig. 3a of the main manuscript). Similarly, considering the nonlinear extension of the uppermost state of the edge band (rightmost green trace), one finds a threshold-less bifurcation from the linear solution at $\bar{\beta} = 1.153$. However, the initially steep slope of this branch decreases somewhat as it penetrates further into the gap between edge and bulk band, indicative of a certain contraction of the mode fields (cf. panels "4"-"6"). Finally, considering the uppermost bulk state as starting point (rightmost blue trace and panels "7"-"9"), its nonlinear extension also merges without power threshold. Note that its initial as well as final slopes are even steeper compared to the nonlinear edge state, indicative of the larger number of contributing lattice sites. As the distance of the nonlinear bulk state from the bulk band increases, the nonlinear bulk state slowly contracts towards the center of the triangular plaquette with an approximately linear scaling between U and $\bar{\beta}$. If one compares the linear sections of the graphs for the corner, edge and bulk states shown here, one finds that their respective slopes indeed mirror the number of principally involved lattice sites (one for the corner state, six for the edge state and nine for the bulk state) visible in panels "2", "5" and "8".

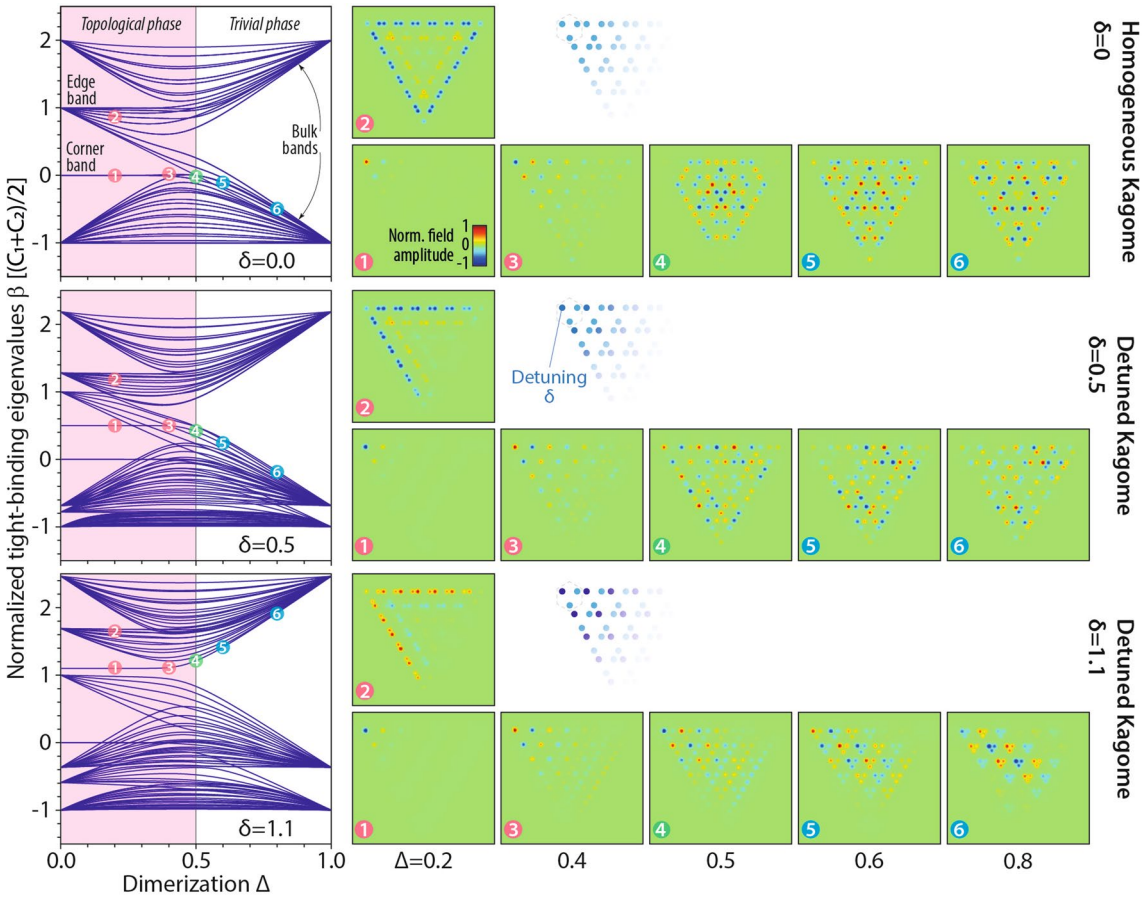


**Extended Data Fig. 2 | Dimerization dependence of the numerically calculated tight-binding eigenvalues of the homogeneous Kagome lattice compared to modified Kagome lattices with detuned upper left waveguide in each unit cell.** Dimerization dependence of the numerically calculated tight-binding eigenvalues of the homogeneous Kagome lattice (top, equivalent to Fig. 1b,c of the main manuscript) compared to modified Kagome lattices where the on-site potential of the upper left waveguide in each unit cell is subject to a detuning of $\delta = 0.5$ (middle) and $\delta = 1.1$ (bottom). In line with the center of the intermediate regime of nonlinear delocalization observed in the strongly dimerized topological system (red plot in Fig. 3a), a detuning of $\delta = 1$ approximately corresponds to a normalized power of 2.0 MW · cm, assuming that the wave packet is confined to a single lattice site. Representative mode profiles corresponding to the marked locations "1"…"6" in each group are shown as panels on the right. While the introduction of a detuning in the upper left waveguide of the unit cell breaks the chiral symmetry of the lattice, and with it the degeneracy of the topological corner- and edge state branches, the topological states themselves persist. For strong detunings $\delta > 1$, the detuned corner state branch generally lies above the undetuned edge band. In contrast, for intermediate detunings, for example $\delta = 0.5$, the branch associated with states in the detuned corner may actually intersect with the edge band that is comprised of states residing along the opposite edge. This spatial separation prevents any interaction of the respective states that might otherwise impact the topological protection.